Alterations of White Matter Connectivity in Preschool Children with Autism Spectrum Disorder

Shi-Jun Li, MD, PhD • Yi Wang, MD • Long Qian, MSc • Gang Liu, MD • Shuang-Feng Liu, MS • Li-Ping Zou, MD • Ji-Shui Zhang, MS • Nan Hu, MS • Xiao-Qiao Chen, MS • Sheng-Yuan Yu, MD • Sheng-Li Guo, MD • Ke Li, MD • Mian-Wang He, MS • Hai-Tao Wu, PhD • Jiang-Xia Qiu, PhD • Lei Zhang, BS • Yu-Lin Wang, MD • Xin Lou, MD • Lin Ma, MD

From the Departments of Medical Instruments (S.J.L.), Stomatology (Y.W.), Radiology (G.L., S.F.L., Y.L.W., X.L., L.M.), Pediatrics (L.P.Z., X.Q.C.), Rehabilitation Medicine (N.H.), Neurology (S.Y.Y., M.W.H.), Neurosurgery (S.L.G.), and Medical Information (L.Z.), Chinese PLA General Hospital, 28th Fuxing Road, Beijing 100853, China; Department of Biomedical Engineering, Peking University, Beijing, China (L.Q.); Department of Neurology, Beijing Children's Hospital of Capital Medical University, Beijing, China (J.S.Z., K.L.); and Department of Neurobiology, Institute of Basic Medical Sciences, Beijing, China (H.T.W., J.X.Q.). Received February 2, 2017; revision requested April 4; revision received December 11; accepted January 2, 2018l **Address correspondence to** L.M. (e-mail: *cjr.malin@vip.163.com*).

Study supported by Beijing Nova Program (2011112, xxjh2015105); National Natural Science Foundation of China (31100714); Translational Medicine Project of PLA General Hospital 2016 (2016TM-001); and the Natural Science Foundation of Beijing Municipality (7162183).

Conflicts of interest are listed at the end of this article.

Radiology 2018; 288:209–217 • **https://doi.org/10.1148/radiol.2018170059** • **Content code:** NR

Purpose: To investigate the topologic architecture of white matter connectivity networks in preschool-aged children with a diagnosis of autism spectrum disorder (ASD) versus typical development (TD).

Materials and Methods: Forty-two participants were enrolled, including 21 preschool children with ASD (14 male children and seven female children; mean age, 4.56 years ± 0.97 [standard deviation]) and 21 children with TD (11 males and 10 females; mean age, 5.13 years ± 0.82). The diagnosis of ASD was determined according to the Diagnostic and Statistical Manual of Mental Disorders Global Assessment of Functioning scores (mean score, 8.00 ± 0.50). All participants underwent diffusion-tensor imaging (DTI) and T2-weighted imaging on a 3-T magnetic resonance system. A graph theoretical analysis was applied to investigate the topologic organization of the brain network including global and local topologic parameters. Statistical analysis was then performed for the comparison between the groups.

Results: Compared with the TD group, children with ASD demonstrated shortened characteristic path length (t_1 = 0.536, t_2 = 0.534, t_3 = 0.523, t_4 = 0.510, and t_5 = 0.501; $P < .05$) and increased global efficiency (t_1 = 0.499, t_2 = 0.497, t_3 = 0.486, t_4 = 0.473, and t_5 = 0.465; $P < .05$) and clustering coefficient (t_1 = 0.673, t_2 = 0.750, t_3 = 0.757, t_4 = 0.738, and t_5 = 0.741; $P < .05$). Significant increases in nodal efficiency were mainly found in left pallidum (0.037 vs 0.032, respectively; $P < .01$) and right caudate nucleus (0.037 vs 0.032, respectively; $P < .01$) of the basal ganglia network.

Conclusion: Significantly altered patterns of global and local brain network topography may underlie the abnormal brain development in preschool children with ASD compared with those who have TD. The identification of altered structural connectivity in basal ganglia and paralimbic-limbic networks may point toward potential imaging biomarkers for preschool-age patients with ASD.

Online supplemental material is available for this article.

Although the underlying pathophysiology and neurologic basis of autism spectrum disorder (ASD) in patients remain unclear, especially in children with ASD (1), altered brain connectivity is a key feature of ASD pathophysiology (2). Recent neuroimaging findings indicate that ASD is associated with atypical brain connectivity, but the specific neuropathologic aberrations in ASD are yet to be determined (3). Multiple studies (3) of functional connectivity identified patterns of both functional hypo- and hyperconnectivity in adults and children with ASD. Diffusion-tensor imaging (DTI) studies (4) of white matter integrity revealed similar atypical connectivity patterns in children and adolescents with ASD. A recent theory that attempts to reconcile the conflicting results in the literature suggests that hyperconnectivity of brain networks may be more characteristic in young children with ASD, whereas hypoconnectivity is more prevalent in adolescents and adults with the disorder compared with individuals with typical development (TD) (5). However, this atypical brain connectivity in ASD has only been observed at regional levels (2,3). Brain connectivity at the network level has not yet been fully investigated, particularly in preschool children with ASD.

The topologic properties of brain networks have been characterized by using graph theory analysis. This is typically achieved through magnetic resonance (MR) imaging and neurophysiologic data, and from both functional and structural perspectives (6). With this framework, DTI has been used to assess white matter connectivity in the brains of individuals with ASD. This approach has also been used to identify how the topologic organization of the brain network is affected by other psychiatric disorders, such as Alzheimer disease, multiple sclerosis, and epilepsy (7).

On the basis of these recent findings, we hypothesized that abnormalities in preschool children with ASD are mainly associated with white matter hyperconnectivity,

Abbreviations

ASD = autism spectrum disorder, DTI = diffusion-tensor imaging, TD = typical development

Summary

Our graph theory analysis of diffusion-tensor imaging data demonstrate a decreased characteristic path length, increased global efficiency, and increased clustering coefficient in childhood autism spectrum disorder compared typical development. Our findings also indicate an altered network organization, especially in the basal ganglia and paralimbic-limbic networks in preschool children with autism spectrum disorder. These altered patterns of global and local topologic properties may underlie the abnormal brain development process in preschool children with autism spectrum disorder and contribute to the neurophysiologic mechanisms involved.

Implication for Patient Care

Preschool children with autism spectrum disorder (ASD) are associated with altered white matter connectivity patterns, specifically with the hyperconnectivity of basal ganglia and paralimbic-limbic networks; these findings may be regarded as the imaging biomarkers and may help guide the precise intervention or treatment in ASD.

specifically in networks involving the basal ganglia and the paralimbic-limbic system because alterations in these networks are closely related to repetitive and stereotyped behaviors, as well as learning and memory impairment. In our study, we attempted to characterize the whole-brain connectivity in children with ASD and in children with TD by using DTI.

Materials and Methods

Participants

The study protocol approved by the Medical Ethics Committee of the Chinese People's Liberation Army General Hospital was fully disclosed to all participants and their guardians, and written informed consent was obtained from each participant's guardian according the provision of the Declaration of Helsinki. Children with ASD and TD were recruited from the Department of Pediatrics of the Chinese People's Liberation Army General Hospital. Twenty-one children with ASD (14 boys and seven girls; mean age, 4.56 years ± 0.97 [standard deviation]) and 21 children with TD (11 boys and 10 girls; mean age, 5.13 years ± 0.82) participated in this study from July 2012 to July 2016. Basic clinical data were recorded for all participants including IQ, birth history, developmental delay, medication history, handedness, and autism-spectrum quotient questionnaire by pediatricians (J.S.Z., with 21 years of experience, X.Q.C., with 8 years of experience, and L.P.Z., with 34 years of experience) with clinical trial forms in a hospital. A diagnosis of ASD was determined according to the Diagnostic and Statistical Manual of Mental Disorders, Autism Behavior Checklist, and Childhood Autism Rating Scale. Twenty-one children with TD were recruited as control participants, and none had a previous history of neurologic or psychiatric problems. All participants had normal or corrected-to-normal vision, and the usage of psychotropic medications was not reported for any of the children. The exclusion criteria included metal implants, psychiatric or neurologic disorders, structural brain abnormalities, and known genetic conditions. MR examinations were interpreted as normal by experienced neuroradiologists (G.L., with 15 years of experience, X.L., with 20 years of experience, and L.M., with 30 years of experience).

MR Imaging Data Acquisition

All participants underwent DTI, which was performed on a 3-T MR imager (Discovery MR750 system; GE Healthcare, Waukesha, Wis) at the Chinese People's Liberation Army General Hospital. Participants were required to lie in the supine position with their head securely fixed by a belt and foam pads to minimize head motion. Also, the imager provided a real-time monitoring software for head movement. The data were deleted when the translation motion was greater than 2 mm or rotation motion greater than 2°. A scout localizer examination was performed first, followed by T2-weighted imaging with conventional axial fast relaxation and a fast spin-echo sequence to rule out major white matter changes, cerebral infarction, or other lesions. The DTI protocol was as follows: repetition time msec/echo time msec, 8000/minimum; 24 diffusion directions; two excitations; *b* value, 800 sec/mm^2; two T2-weighted images; acquisition matrix, 112 × 112; field of view, 224 × 224 mm; section thickness, 2.0 mm; 0-mm gap; 64 sections. Thereafter, a spatially matched sagittal three-dimensional fast spoiled gradient-echo image was acquired for the reconstruction images to ensure identical distortion characteristics for registration purposes. The three-dimensional fast spoiled gradient-echo imaging parameters applied were as follows: minimum echo time; inversion time msec, 450; one echo; flip angle, 12°; location per slab, 160; acquisition matrix, 240 × 240; field of view, 240 × 240 mm; section thickness, 1.0 mm; no overlap locations.

Image Preprocessing

Eddy current and motion artifacts in the DTI data were corrected by using FMRIB Diffusion Toolbox (FSL, version 4.1; *http://www.fmrib.ox.ac.uk/fsl*). The diffusion-tensor models were then estimated by the linear least-squares fitting method at each voxel by using the Diffusion Toolkit (TrackVis, Charlestown, Mass, *http://trackvis.org/faq/#faq6*). For each participant, whole-brain fiber tracking was performed in native diffusion space via the fiber assignment by continuous tracking algorithm with TrackVis software. All the tracts in the TrackVis dataset were computed by seeding each voxel with a fractional anisotropy (FA) larger than 0.2. Tractography was terminated if it turned at an angle exceeding 45° or reached a voxel with a fractional anisotropy less than 0.2 (8).

Network Construction

Nodes and edges are the two basic elements needed to form a network. Brain white matter connectivity was modeled as a network composed of a total of 90 nodes (Table 1). To construct a structural connectivity network in each participant, the region-of-interest nodes were defined in the native diffusion space as previously described and identified by using software (SPM8; *http://www.fil.ion.ucl.ac.uk/spm/software/ spm8*). Specifically, individual T1-weighted images were co-registered to the B_0 images in the DTI space, and the transformed T1-weighted images were then nonlinearly transformed into the ICBM152 T1 template from

the Montreal Neurologic Institute database (9). Inverse transformations were applied to warp the Automated Anatomic Labeling atlas from the Montreal Neurologic Institute space to the DTI native space. To define the respective network edges of the 90 regions surrounding the 90 nodes, a threshold value was selected for the fiber bundles as previously described (8). Two regions were considered structurally connected if three or more fiber bundles with two endpoints were located in these two regions. In addition, we evaluated the effects of different thresholds on the network analysis by setting threshold values of fiber bundles from 1 to 5. It was observed that changing the threshold values did not significantly influence the results. If not indicated otherwise, we report our results based on a threshold value of 3. Moreover, we defined the fiber number of the connected fibers between two regions as the weights of the network edges. As a result, a fiber-number–weighted white matter network for each participant was constructed and represented by a symmetric 90 × 90 matrix.

Table 1: Cortical and Subcortical Regions of Interest Defined in the Study

Index	Region	Abbreviation
(1,2)	Precentral gyrus	PreCG
(3,4)	Superior frontal gyrus, dorsolateral	SFGdor
(5,6)	Superior frontal gyrus, orbital part	ORBsup
(7,8)	Middle frontal gyrus	MFG
(9,10)	Middle frontal gyrus, orbital part	ORBmid
(11,12)	Inferior frontal gyrus, opercular part	IFGoperc
(13,14)	Inferior frontal gyrus, triangular part	IFGtriang
(15,16)	Inferior frontal gyrus, orbital part	ORBinf
(17,18)	Rolandic operculum	ROL
(19,20)	Supplementary motor area	SMA
(21,22)	Olfactory cortex	OLF
(23,24)	Superior frontal gyrus, medial	SFGmed
(25,26)	Superior frontal gyrus, medial orbital	ORBsupmed
(27,28)	Gyrus rectus	REC
(29,30)	Insula	INS
(31,32)	Anterior cingulate and paracingulate gyri	ACG
(33,34)	Median cingulate and paracingulate gyri	DCG
(35,36)	Posterior cingulate gyrus	PCG
(37,38)	Hippocampus	HIP
(39,40)	Parahippocampal gyrus	PHG
(41,42)	Amygdala	AMYG
(43,44)	Calcarine fissure and surrounding cortex	CAL
(45,46)	Cuneus	CUN
(47,48)	Lingual gyrus	LING
(49,50)	Superior occipital gyrus	SOG
(51,52)	Middle occipital gyrus	MOG
(53,54)	Inferior occipital gyrus	IOG
(55,56)	Fusiform gyrus	FFG
(57,58)	Postcentral gyrus	PoCG
(59,60)	Superior parietal gyrus	SPG
(61,62)	Inferior parietal lobule, but supramarginal and angular gyri	IPL
(63,64)	Supramarginal gyrus	SMG
(65,66)	Angular gyrus	ANG
(67,68)	Precuneus	PCUN
(69,70)	Paracentral lobule	PCL
(71,72)	Caudate nucleus	CAU
(73,74)	Lenticular nucleus, putamen	PUT
(75,76)	Lenticular nucleus, pallidum	PAL
(77,78)	Thalamus	THA
(79,80)	Heschl gyrus	HES
(81,82)	Superior temporal gyrus	STG
(83,84)	Temporal pole: superior temporal gyrus	TPOsup
(85,86)	Middle temporal gyrus	MTG
(87,88)	Temporal pole: middle temporal gyrus	TPOmid
(89,90)	Inferior temporal gyrus	ITG

Note.—Data in parentheses are index numbers that indicate left hemisphere and right hemisphere. The regions are listed according to a prior template obtained from an Automated Anatomic Labeling atlas. Odd numbers represent the corresponding brain regions in the left hemisphere and even numbers indicate those in the right hemisphere.

Global Topologic Parameters

Previous studies (10) demonstrated two key metrics for describing the complex networks in the human brain: the clustering coefficient (*Cp*) and characteristic path length (*Lp*). To investigate the small-world properties, *Cp* and *Lp* were compared with those of the corresponding random networks (10). Generally, a small-world network will demonstrate a significantly higher clustering coefficient value than that of a random network ($\gamma = Cp_{(real)}/Cp_{(rand)} > 1$), where *real* is real network and *rand* is random network, whereas the characteristic path length will be comparable to those of random networks ($\lambda = Lp_{(real)}/Lp_{(rand)} \sim 1$) (10). These two measurements can be collectively reflected by a simple quantitative metric, small-worldness, which is described as $\sigma = \gamma/\lambda$. Small-worldness is typically greater than 1 for small-world networks. In the current study, the network strength, *S(G)*, global efficiency, $E_{glob}(G)$, and local efficiency, $E_{loc}(G)$, of a network G were investigated as well. The network strength refers to the average of the edge weights linking to a specific node across all nodes (8). $E_{glob}(G)$ measures the global efficiency of the parallel information transfer in the network, whereas $E_{loc}(G)$ reveals the fault tolerance of the network, which indicates the efficiency of communication among the first neighbors of *i* when *i* is removed (10). Notably, in our study, estimations of all parameters were under consideration of weighted coefficients, which was consistent with a previous study. The estimations of all parameters were calculated by using the code provided by the Brain Connectivity Toolbox (11).

Regional Nodal Characteristics

Generally speaking, there are three common nodal characteristics: nodal degree, nodal betweenness, and nodal efficiency. In our study, we computed the corresponding regional efficiencies (E_i^w) to determine the nodal (regional) characteristics of white matter connectivity brain networks as described previously (8). The regional efficiency we defined as the inverse of the shortest mean of the harmonic path length between the target node and all other nodes in the network (8,10). The nodes with an E_i^w that were at least one standard deviation larger than the average for the network were considered to be hubs (12).

Table 2: Demographic and Neuropsychologic Characteristics of TD and ASD Groups

Characteristics	ASD	TD	*P* Value*
Mean age (y)†	4.56 ± 0.97	5.13 ± 0.82	.040
Sex (no. of patients)			.268
Male	14	11	
Female	7	10	
IQ score range per WPPSI	89–100	90–110	.132
Handedness (no. of patients)			>.999
Right	20	21	
Left	1	0	
DSM score†	8.00 ± 0.50	…	…
ABC score †	56.00 ± 7.42	…	…
CARS score ‡	31.0 (0)	15.0 (0)	<.001
Verbal communication	3 (0)	1 (0)	<.001
Object use	2 (1)	1 (0)	<.001
Visual response	2 (0)	1 (0)	<.001
Body use	2 (0)	1 (0)	<.001
Listening response	2 (0)	1 (0)	<.001

Note—ABC = Autism Behavior Checklist, ASD = autism spectrum disorder, CARS = Childhood Autism Rating Scale, DSM = Diagnostic and Statistical Manual of Mental Disorders Global Assessment of Functioning, TD = typical development, WPPSI = Wechsler Preschool and Primary Scale of Intelligence.

* The *P* value for the intergroup age difference was obtained by *t* test. The *P* value for the intergroup sex distribution was obtained by using a χ^2 test. The *P* value for the intergroup IQ distribution was obtained by using a Kolmogorov-Smirnov *Z* test. The *P* value for the intergroup handedness was obtained by using a Fisher exact test. The *P* value for the Childhood Autism Rating Scale was obtained by using Wilcoxon test.

† Data are mean ± standard deviation.

‡ Data are median; data in parentheses are interquartile range.

Network Connectivity Characteristics

To further localize specific pairs of brain regions in which the structural connectivity was altered in children with ASD, we used a network-based-statistic approach (13). Specifically, we first identified regional pairs, which showed between-group differences in structural connectivity, and then used the network-based-statistic method to localize connected networks that showed significant changes in childhood ASD.

Statistical Analysis

An independent sample *t* test was applied to investigate the differences between ASD and TD groups for each variable measured on a scale, such as age, whereas a χ^2 test was used to explore the same differences for each categorical variable. Pairwise comparisons were performed by using a linear model to determine intergroup differences in global network measurements and regional topologic profile (90 nodes). We adjusted for the effects of demographic characteristics, such as age and sex, in all analyses by performing a regression analysis before the statistical analysis of structural connections. In addition, to control the error of multiple comparisons among those five thresholds in global network measurements or those 90 nodes in regional topologic profile, a false-discovery rate method performed at a *P* value of .05 or less was considered to indicate statistical significance in our results. To determine the significance levels of altered connectivity networks in the network-based-statistic analysis, we first detected significant nonzero connections within each group by performing a nonparametric one-tailed sign test (corrected by using the Bonferroni method at $P < .05$; $90 \times 89/2 = 4005$ pairs of regions). Next, nonzero connections within either the ASD or TD group were identified and combined into a connection mask for that group. The network-based statistic approach was then conducted within the connection mask, where a primary threshold ($P < .05$) was first applied to a *t* statistic (two-sample one-tailed *t*-tests). To estimate the significance for each component, the nonparametric permutation approach (10 000 permutations) was performed. Finally, a threshold of $P < .05$ was used to generate supra threshold links, among which the maximal connected component size was recorded (13).

Results

Demographic and Neuropsychologic Results

The demographic data and neuropsychologic characteristics for children with ASD and TD are shown in Table 2. There was no significant intergroup difference in age (*t* test, $P = .040$), sex (χ^2 test, $P = .268$), IQ (Kolmogorov-Smirnov *Z* test, $P = .132$, two-tailed), and handedness (*F* test, $P > .999$), whereas there was significant between-group difference in Childhood Autism Rating Scale and its five items ($P < .001$).

Global Topologic Alterations in ASD

Overall group mean global topologic patterns (network strength, global and local efficiency, characteristic path length *Lp*, clustering coefficient *Cp*, λ, γ, and σ) are shown in Figure 1 as a function of the threshold *n* (range from 1 to 5), where

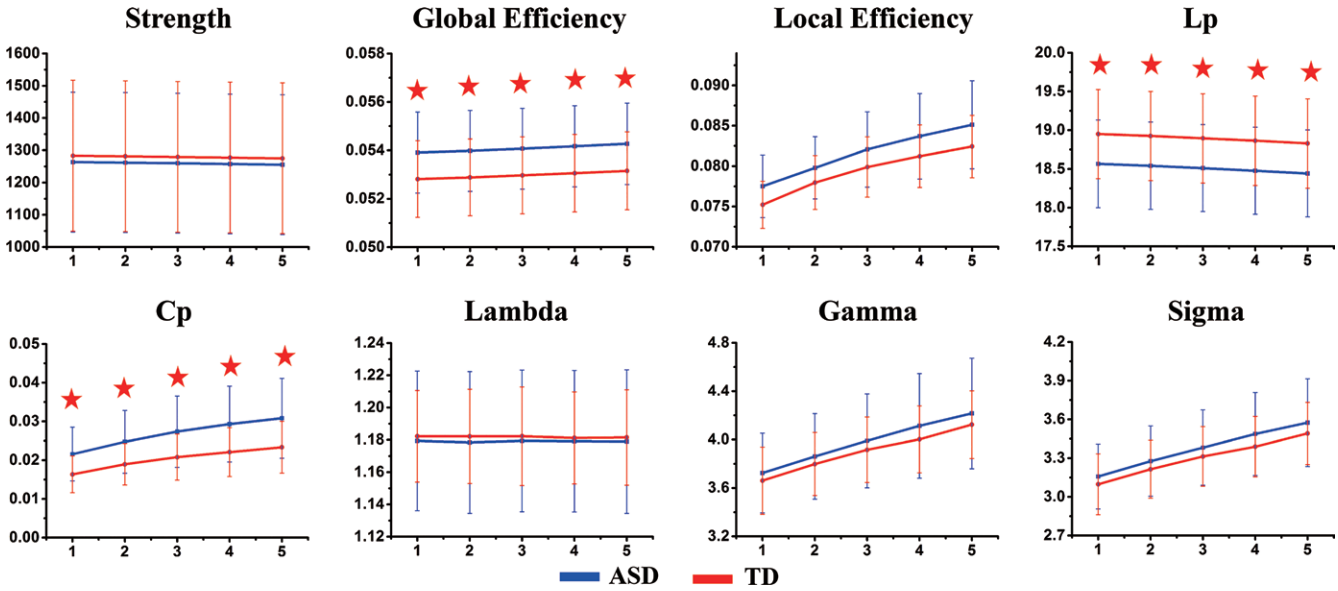

Figure 1: Global measurements of white matter connectivity networks in typical development (TD) and autism spectrum disorder (ASD) groups. The threshold *T* (x-axis) determined the minimum streamlines required to interconnect a pair of nodes for a connection to be assumed. *T* = n (1, 2, 3, 4, 5) indicates that the minimum number of streamlines required for a link to be drawn. Significant between-group differences (red star; $P < .05$, corrected) were found for global efficiency, characteristic path length (Lp), and clustering coefficients (Cp), and for all thresholds.

n represents the minimum number of streamlines required to interconnect a pair of nodes for a connection to be assumed. Both the ASD and TD groups demonstrated a small-world organization of white matter networks, as expressed by γ larger than 1, λ approximately 1, and σ larger than 1 (Fig 1).The ASD group displayed a decreased characteristic path length, and increased global efficiency and clustering coefficient compared with the TD group (Fig 1; $P < .05$, false discovery rate corrected). No significant differences were observed between the two groups in other global topologic patterns.

Nodal Characteristics in Identification of Network Hubs for Each Group

The nodes identified as hubs are shown in Figure 2 and Table 3. We found several common nodes that showed network hub properties for both groups. Specifically, 12 consistent hub regions were identified in both groups: the bilateral supplementary motor area, middle temporal gyrus, precuneus, right postcentralgyrus, precentralgyrus, dorsolateral superior frontal gyrus, middle frontal gyrus, superior temporal gyrus, and right inferior temporal gyrus. However, the left medial part of the superior frontal gyrus was identified as a hub in the TD group only, whereas the left middle occipital gyrus and left inferior temporal gyrus were identified as hubs in the ASD group only.

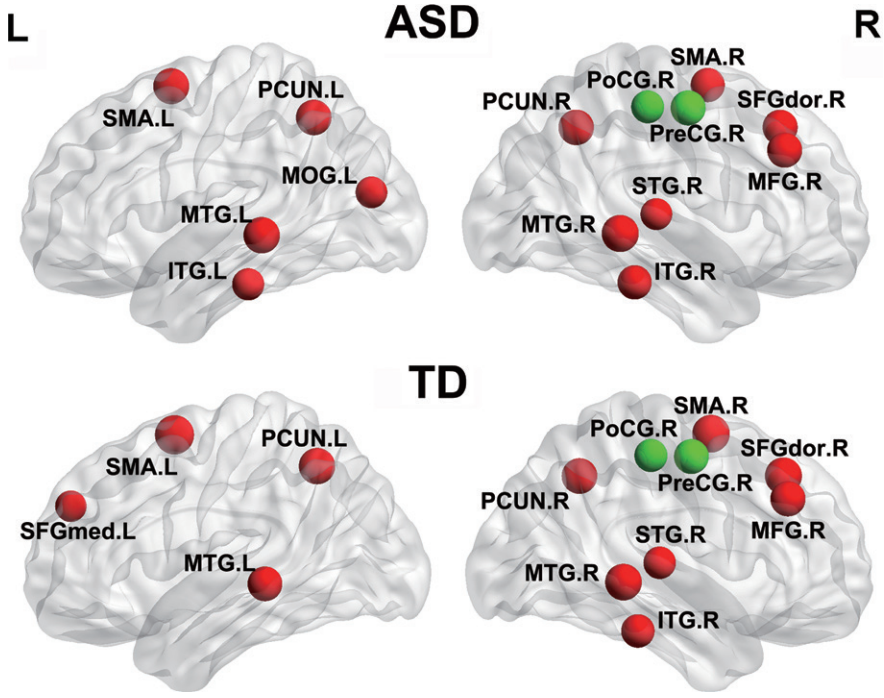

Figure 2: The distribution of hub regions in typical development (TD) and autism spectrum disorder (ASD) groups. Hub regions were visualized by using the BrainNet viewer (NKLCNL; Beijing Normal University, *www.nitrc.org/projects/bnv/*). Hub regions were defined as nodes with regional efficiencies at least one standard deviation higher than the average for the network by using three-dimensional rendering maps. These areas included association (red) and primary (green) regions. Please see Table 1 for abbreviations of these regions. L = left; R = right.

Intergroup Difference in Regional Efficiency

In addition to discovering characteristic global network organization in ASD, an intergroup comparison of regional efficiency also showed alterations in brain regions of children with ASD. The results were demonstrated in Figure 3 and Table 4

. Of the 90 tested regions, 16 regions with a *P* value less than .05 were included in this study, and only two brain regions, the left pallidum and the right caudate, demonstrated a *P* value of less than .05 corrected with false discovery rate. Three colors (red, magenta, and blue) were used to represent *P* values of nodes less than .05 ($P < .05$, false discovery rate corrected), less than .01 ($P < .01$, uncorrected), and less than .05 ($P < .05$, uncorrected), respectively (Fig 3).

Compared with the TD group, a significant increase in nodal efficiency of ASD group was found in the basal ganglia network including bilateral caudate (left caudate: 0.037 vs 0.035, $P = .044$; right caudate: 0.037 vs 0.032, $P < .001$), putamen (left putamen: 0.062 vs 0.056, $P = .022$; right putamen: 0.061 vs 0.055, $P = .029$), pallidum (left pallidum: 0.037 vs 0.032, $P < .001$; right palladium: 0.034 vs 0.030, $P = .008$) and in the paralimbic-limbic network including bilateral hippocampus (left hippocampus: 0.038 vs 0.034, $P = .019$; right hippocampus: 0.049 vs 0.043, $P = .012$), parahippocampal gyrus (left parahippocampal gyrus: 0.046 vs 0.042, $P = .019$; right parahippocampal gyrus: 0.052 vs 0.048, $P = .005$), left temporal pole of superior temporal gyrus (0.043 vs 0.039, $P = .019$) and right amygdala (0.033 vs 0.028, $P = .034$). Similarly, a significant increase in nodal efficiency was observed in the left Heschl gyrus (0.032 vs 0.027, $P = .021$) and bilateral fusiform gyrus (left fusiform gyrus: 0.062 vs 0.059, $P = .003$; right fusiform gyrus: 0.065 vs 0.062, $P = .042$). Right supplementary motor area (0.073 vs 0.081, $P = .049$) was the only region that displayed a decreased nodal efficiency pattern in the ASD group (Table 4).

Connectivity-based Analysis

A node-based network-based-statistic method was used to identify the characteristic connected components in ASD (Fig 4). A single connected network with 13 nodes and 12 connections in the left hemisphere was altered in the ASD group compared with the TD group (Bonferroni-corrected $P = .036$). The nodal regions involved in this network were located in the paralimbic-limbic network, including the left medial orbital of the superior frontal gyrus, orbital part of the superior frontal gyrus, orbital part of the inferior frontal gyrus, gyrus rectus, anterior cingulate gyrus, olfactory cortex, temporal pole of superior temporal gyrus, hippocampus, and parahippocampal gyrus, and in the occipital system, including the left fusiform gyrus, lingual gyrus, middle occipital gyrus, and inferior occipital gyrus. Compared with the TD group, ASD showed only increased connec-

Table 3: Hub Regions of White Matter Networks in TD and ASD Groups

Hub Region	Mean TD E_{nodal}	Mean ASD E_{nodal}	Class
SMA.L	0.08386	0.07704	Association
SMA.R	0.08054	0.07324	Association
SFGdor.R	0.07917	0.07506	Association
MTG.L	0.07409	0.07762	Association
MTG.R	0.07822	0.07912	Association
PCUN.L	0.07774	0.07603	Association
PCUN.R	0.07619	0.07597	Association
MFG.R	0.07517	0.07487	Association
PreCG.R	0.07447	0.07496	Primary
ITG.R	0.07158	0.07309	Association
PoCG.R	0.07063	0.07029	Primary
STG.R	0.06938	0.06788	Association
SFGmed.L	0.06717	…	Association
ITG.L	…	0.06874	Association
MOG.L	…	0.06797	Association

Note.—The fiber number–weighted white matter network for each participant was constructed by using an Automated Anatomic Labeling template. The hub regions were identified if E_i^w was at least one standard deviation larger than the average nodal efficiency of the network. The hubs were then sorted by the mean nodal efficiency in each group. The cortical regions were classified as primary or association areas. E_{nodal} = nodal efficiency, ITG = inferior temporal gyrus, L = left, MFG = middle frontal gyrus, MOG = middle occipital gyrus, MTG = middle temporal gyrus, PCUN = precuneus, PoCG = postcentralgyrus, PreCG = precentralgyrus, R = right, SFGdor = dorsolateral superior frontal gyrus, SFGmed = medial superior frontal gyrus, SMA = supplementary motor area, STG = superior temporal gyrus.

Table 4: Differences in Nodal Efficiency between TD and ASD Groups

Region	Functional Classification	ASD Group	TD Group	*P* Value
PAL.L	Subcortical	0.03698	0.03186	.0007
CAU.R	Subcortical	0.03734	0.03195	.0009
FFG.L	Association	0.06210	0.05873	.0034
PHG.R	Paralimbic	0.05232	0.04788	.0049
PAL.R	Subcortical	0.03371	0.02973	.0082
HIP.R	Limbic	0.04891	0.04339	.0119
PHG.L	Paralimbic	0.04611	0.04231	.0186
TPOsup.L	Paralimbic	0.04335	0.03930	.0186
HIP.L	Limbic	0.03822	0.03398	.0191
HES.L	Primary	0.03214	0.02675	.0207
PUT.L	Subcortical	0.06166	0.05587	.0222
PUT.R	Subcortical	0.06083	0.05512	.0287
AMYG.R	Subcortical	0.03254	0.02847	.0337
FFG.R	Association	0.06487	0.06174	.0419
CAU.L	Subcortical	0.03717	0.03516	.0441
SMA.R	Association	0.07324	0.08054	.0493

Note.—Of the 90 tested regions in Table 1, 16 regions with *P* value less than .05 were included. The fiber number–weighted white matter network for each participant was constructed by using an Automated Anatomic Labeling template. Between-group comparisons of nodal efficiency were performed by using a multivariable regression analysis in which the effects of age and sex were controlled. AMYG = amygdala, CAU = caudate, FFG = fusiform gyrus, HES = Heschl gyrus, HIP = hippocampus, L = left, PAL = palladium, PHG = parahippocampal gyrus, PUT = putamen, R = right, SMA = supplementary motor area, TPOsup = temporal pole of superior temporal gyrus.

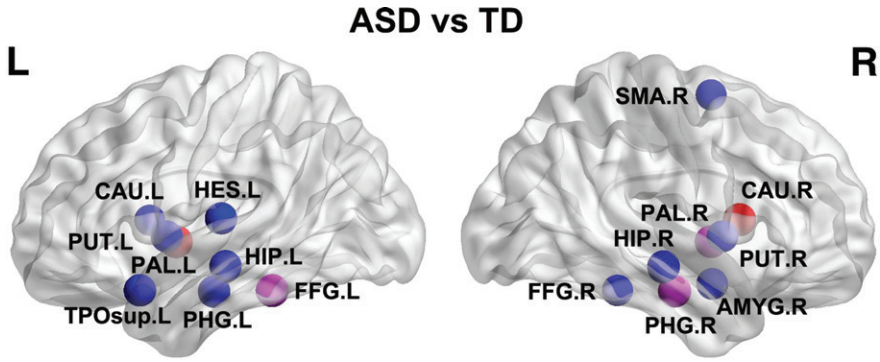

Figure 3: Brain regions with significant between-group differences in nodal efficiency. Nodes represent brain regions with significant intergroup differences in the regional efficiencies (corrected and uncorrected). Brain regions are shown in red, purple, and blue and indicate nodal *P* values that are, respectively, $P < .05$ (false discovery rate corrected), $P < .01$ (uncorrected), and $P < .05$ (uncorrected). ASD = autism-spectrum disorder; L = left; R = right; TD = typical development. See Table 1 for region abbreviations.

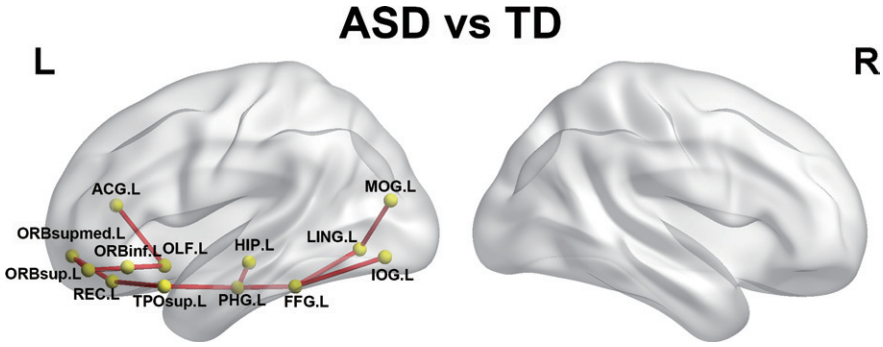

Figure 4: Networks showing increased structural connections in children with autism-spectrum disorder (ASD) compared with children with typical development (TD). The regional pairs showed increased connections in children with ASD compared with TD. These connections formed a single connected network with 13 nodes and 12 connections in the left (L) hemisphere ($P = .0358$, corrected). The fiber number–weighted white matter network for each participant was constructed by using the Automated Anatomic Labeling template. The nodes and connections were mapped onto the cortical surfaces by using the brain network visualization tool BrainNet viewer (NKLCNL; Beijing Normal University). R = right. See Table 1 for region abbreviations.

tions in those nodal regions (Table 4). Moreover, the connectivity differences between the ASD and TD groups were only observed in the left hemisphere (Fig 4).

Discussion

By using DTI in combination with graph theory methods, we demonstrated topologic alterations of white matter networks in preschool children with ASD. Our results demonstrated that there were correlations between the white matter networks topologic alterations (with significant topologic alterations in the basal ganglia and paralimbic-limbic network) and the clinical scales (with significant differences in verbal communication, object use, visual response, body use, and listening response from Childhood Autism Rating Scale). The results suggest delayed or stunted maturation processes, including repetitive and stereotyped behaviors (body use), aberrant observation (visual response) and imitation capacity (object use), language deficits and delayed language development (verbal communication), the atypical face perception, abnormal auditory function (listening response), and motor dysfunction (body use) in preschool children with ASD. First, global topologic patterns of white matter networks in children with ASD were significantly altered, as indicated by a decreased characteristic path length, increased global efficiency, and an increased clustering coefficient compared with children with TD. Second, nodes with significant topologic alterations were mainly distributed in the basal ganglia network, including the bilateral caudate, putamen, and pallidum, and in the paralimbic-limbic network, including the bilateral hippocampus, parahippocampal gyrus, left temporal pole of the superior temporal gyrus, and right amygdala. Third, significantly altered white matter connectivities were located in the left hemisphere, which might provide support for the left-hemisphere hypothesis for autism (14). These findings extend our understanding of the neurophysiologic mechanisms involved in ASD from a network perspective.

Our results demonstrate that global network measures (ie, γ and λ) had a small-world organization of white matter networks in both ASD and TD, which is consistent with the findings of previous studies (15). Several topologic profiles were significantly altered in children with ASD (specifically, characteristic path length, global efficiency, and clustering coefficient), which suggests hyperconnectivity in the brains of ASD children and confirms previous observations from neuroimaging studies (2,5). The high brain connectivity revealed in childhood ASD in our study may be indicative of the earliest signs of abnormal brain development in autism. For example, children with ASD on average display enlarged head circumference or macrocephaly (16). In addition, infants and young children with ASD can show early brain overgrowth (17), and an excess number of neurons in the prefrontal cortex, as revealed by postmortem studies (2). On the basis of these previous results and those of our current study, we argue that the global hyperconnectivity in brains of children with ASD might be one of the underlying mechanisms for the abnormal brain development observed in ASD.

Regarding nodal properties, we found a striking predominance of increased nodal efficiency in childhood ASD compared with TD, which is in agreement with previous studies in adults (2,3). This brain hyperconnectivity in childhood ASD has been interpreted as a reflection of the delayed or stunted maturation processes (18). In addition, our results highlight the critical role of nodes in the basal ganglia network and paralimbic-limbic system in childhood ASD. Abnormal nodes in the basal ganglia

network have been used to explain the repetitive and stereotyped behaviors in children with ASD (19). Likewise, the implication of paralimbic-limbic areas is consistent with studies highlighting ASD-related dysfunction within higher order circuits subserving social, cognitive, and affective processes. In particular, abnormal activity has been reported in specialized regions, such as the temporal poles (20), the hippocampus and parahippocampal gyrus for learning and memory (21), and the amygdale for emotion processing (22). Furthermore, the increased efficiency we observed in the fusiform gyrus may contribute to the atypical face perception in ASD, as indicated previously (23). The observed intergroup difference in Heschl gyrus can be attributed to the abnormal auditory function in ASD on the basis of these recent findings (24). Heschl gyrus contains the primary auditory cortex and plays a critical role in early auditory processing (25).

Conversely, we also observed areas of decreased nodal efficiency. The observed decrease in the nodal efficiency in the supplementary motor area in ASD may be associated with motor dysfunction. Specifically, the weak connection detected between the left ventral premotor cortex and the supplementary motor area may indicate an impaired speech production network in ASD (26). A previous study conducted with a sequential finger-tapping task also showed significant differences between individuals with TD and ASD in the brain network regions involved in motor execution (27). Whereas the observed increase in connections between the paralimbic-limbic system and the occipital network demonstrated the important role of the paralimbic-limbic network in childhood ASD, disconnections between these networks may be associated with an aberrant observation and imitation capacity in childhood ASD (28). In addition, our observations were consistent with the left hemisphere hypothesis for autism, which provides explanations for many symptoms of autism, such as language deficits and delayed language development (14).

Compared with the control group, higher fractional anisotropy values were observed in children with ASD in the corpus callosum, posterior cingulated cortex, and limbic lobes. The converging findings may be involved in behavioral and cognitive deficits associated with ASD, especially in the early age of 2–3-year-old toddlers (29). Tractography analysis in 61 adult men showed increased mean and perpendicular diffusivity, and reduced number of streamlines in the anterior and long segments of the arcuate fasciculus, cingulum, and uncinate in the left hemisphere; and the abnormalities in the anterior portions of the corpus callosum connecting left and right frontal lobes. As long association fibers, the arcuate and uncinate fasciculus connect the frontal lobes with the temporal lobes (30). Thus, significant increases in nodal efficiency of the left temporal pole of superior temporal gyrus may be related to alterations of the arcuate and uncinate fasciculi. The degree of microstructural alterations of the arcuate and uncinate fasciculi was associated with severity of symptoms in language and social reciprocity in childhood.

The sensitivity to environmental cues influences children's ability to suppress thoughts and actions; control systems might be dominated by a primitive limbic system, rendering control systems unable to appropriately modulate behavior. Four-year-old children had more difficulty than did adults in suppressing responses to temptation with the normal limbic system (31). But if the nodal efficiency of paralimbic-limbic network was found significantly increased in the ASD group, the children may show more suppressing responses and resist the temptation. This kind of increased suppression may conceal their original ability to communicate and interact with others, and the ASD children may not recollect their temptation when the paralimbic-limbic network works in excess. Thus, the network disorder of paralimbic-limbic may be related to less communication of ASD.

There are several limitations in this study. First, the number of diffusion gradients directions used in this study was relatively limited. This was primarily because of the constrained imaging time in preschool children with ASD. Second, this study may face the challenge of crossing or so-called kissing fibers because of the constrained b value and the conventional tractography analysis method adopted. Higher b values potentially allow for more sensitive probing of the fiber microstructures by promoting the diffusion level. Methods such as probabilistic tractography to define network edges (32) may be exercised to alleviate these issues. Third, the analysis of node definitions was limited to Automated Anatomic Labeling (Montreal Neurologic Institute) template–based brain networks. Previous studies (33) suggested that the topologic organization of brain networks could be affected by different parcellation strategies. Future studies are therefore required to clarify the effect of various node definitions. Finally, the limited sample size did not allow for the verification of split-half analysis. Autism-spectrum quotient questionnaire, verbal fluency, and comprehension may all be confounders with varying significance levels for preschool children. In addition, clinical conditions including developmental milestones, birth history, and prematurity may also play the role of confounders given the focus on neuronal connectivity in the pediatric population. Larger cohorts in future studies may allow for the verification of the findings among groups with different clinical conditions.

In conclusion, our graph theory analysis of DTI data demonstrates a decreased characteristic path length, increased global efficiency, and increased clustering coefficient in childhood ASD compared with TD. Our findings also indicate an altered network organization, especially in the basal ganglia and paralimbic-limbic networks in preschool children with ASD. These altered patterns of global and local topologic properties may underlie the abnormal brain development process in preschool children with ASD and contribute to the neurophysiologic mechanisms involved.

Author contributions: Guarantors of integrity of entire study, S.J.L., Y.W., L.Q., G.L., S.F.L., L.P.Z., J.S.Z., N.H., S.L.G., M.W.H., J.X.Q., X.L., L.M.; study concepts/study design or data acquisition or data analysis/interpretation, all authors; manuscript drafting or manuscript revision for important intellectual content, all authors; approval of final version of submitted manuscript, all authors; agrees to ensure any questions related to the work are appropriately resolved, all authors; literature research, S.J.L., L.Q., S.Y.Y., M.W.H., H.W., X.L.; clinical studies, S.J.L., Y.W., L.Q., G.L., S.F.L., L.P.Z., J.S.Z., N.H., X.Q.C., S.Y.Y., S.L.G., K.L., M.W.H., Y.L.W., X.L.; experimental studies, S.J.L., L.Q., S.F.L., S.Y.Y., M.W.H., X.L.; statistical analysis, S.J.L., L.Q., S.Y.Y., M.W.H., J.X.Q.; and manuscript editing, S.J.L., L.Q., S.Y.Y., M.W.H., H.W., L.Z., L.M.

Disclosures of Conflicts of Interest: **S.J.L.** disclosed no relevant relationships. **Y.W.** disclosed no relevant relationships. **L.Q.** disclosed no relevant relationships. **G.L.** disclosed no relevant relationships. **S.F.L.** disclosed no relevant relationships.

L.P.Z. disclosed no relevant relationships. **J.S.Z.** disclosed no relevant relationships. **N.H.** disclosed no relevant relationships. **X.Q.C.** disclosed no relevant relationships. **S.Y.Y.** disclosed no relevant relationships. **S.L.G.** disclosed no relevant relationships. **K.L.** disclosed no relevant relationships. **M.W.H.** disclosed no relevant relationships. **H.T.W.** disclosed no relevant relationships. **J.X.Q.** disclosed no relevant relationships. **L.Z.** disclosed no relevant relationships. **Y.L.W.** disclosed no relevant relationships. **X.L.** disclosed no relevant relationships. **L.M.** disclosed no relevant relationships.

References

1. Courchesne E, Mouton PR, Calhoun ME, et al. Neuron number and size in prefrontal cortex of children with autism. JAMA 2011;306(18):2001–2010.
2. Supekar K, Uddin LQ, Khouzam A, et al. Brain hyperconnectivity in children with autism and its links to social deficits. Cell Reports 2013;5(3):738–747.
3. Di Martino A, Yan CG, Li Q, et al. The autism brain imaging data exchange: towards a large-scale evaluation of the intrinsic brain architecture in autism. Mol Psychiatry 2014;19(6):659–667.
4. Spurgin AA. Diffusion Tensor Imaging in Children and Adolescents: A Technology Review. Stanford J Neurosci 2007;1(1):15–17.
5. Nomi JS, Uddin LQ. Developmental changes in large-scale network connectivity in autism. Neuroimage Clin 2015;7:732–741.
6. Bullmore ET, Bassett DS. Brain graphs: graphical models of the human brain connectome. Annu Rev Clin Psychol 2011;7(1):113–140.
7. van den Heuvel MP, Fornito A. Brain networks in schizophrenia. Neuropsychol Rev 2014;24(1):32–48.
8. Bai F, Shu N, Yuan Y, et al. Topologically convergent and divergent structural connectivity patterns between patients with remitted geriatric depression and amnestic mild cognitive impairment. J Neurosci 2012;32(12):4307–4318.
9. Tzourio-Mazoyer N, Landeau B, Papathanassiou D, et al. Automated anatomical labeling of activations in SPM using a macroscopic anatomical parcellation of the MNI MRI single-subject brain. Neuroimage 2002;15(1):273–289.
10. Liu Y, Duan Y, He Y, et al. Altered topological organization of white matter structural networks in patients with neuromyelitis optica. PLoS One 2012;7(11):e48846.
11. Zhang Z, Liao W, Chen H, et al. Altered functional-structural coupling of large-scale brain networks in idiopathic generalized epilepsy. Brain 2011;134(Pt 10):2912–2928.
12. Hosseini SM, Hoeft F, Kesler SR Sr. GAT: a graph-theoretical analysis toolbox for analyzing between-group differences in large-scale structural and functional brain networks. PLoS One 2012;7(7):e40709.
13. Zalesky A, Fornito A, Bullmore ET. Network-based statistic: identifying differences in brain networks. Neuroimage 2010;53(4):1197–1207.
14. DeLong GR. Autism: new data suggest a new hypothesis. Neurology 1999;52(5):911–916.
15. Shi F, Wang L, Peng Z, Wee CY, Shen D. Altered modular organization of structural cortical networks in children with autism. PLoS One 2013;8(5):e63131.
16. Lainhart JE, Piven J, Wzorek M, et al. Macrocephaly in children and adults with autism. J Am Acad Child Adolesc Psychiatry 1997;36(2):282–290.
17. Courchesne E, Carper R, Akshoomoff N. Evidence of brain overgrowth in the first year of life in autism. JAMA 2003;290(3):337–344.
18. Di Martino A, Kelly C, Grzadzinski R, et al. Aberrant striatal functional connectivity in children with autism. Biol Psychiatry 2011;69(9):847–856.
19. Estes A, Shaw DW, Sparks BF, et al. Basal ganglia morphometry and repetitive behavior in young children with autism spectrum disorder. Autism Res 2011;4(3):212–220.
20. O'Nions E, Sebastian CL, McCrory E, Chantiluke K, Happé F, Viding E. Neural bases of Theory of Mind in children with autism spectrum disorders and children with conduct problems and callous-unemotional traits. Dev Sci 2014;17(5):786–796.
21. Zalla T, Sperduti M. The amygdala and the relevance detection theory of autism: an evolutionary perspective. Front Hum Neurosci 2013;7:894.
22. Dalton KM, Nacewicz BM, Johnstone T, et al. Gaze fixation and the neural circuitry of face processing in autism. Nat Neurosci 2005;8(4):519–526.
23. Pierce K, Redcay E. Fusiform function in children with an autism spectrum disorder is a matter of "who". Biol Psychiatry 2008;64(7):552–560.
24. Roberts TP, Cannon KM, Tavabi K, et al. Auditory magnetic mismatch field latency: a biomarker for language impairment in autism. Biol Psychiatry 2011;70(3):263–269.
25. Galaburda A, Sanides F. Cytoarchitectonic organization of the human auditory cortex. J Comp Neurol 1980;190(3):597–610.
26. Peeva MG, Tourville JA, Agam Y, Holland B, Manoach DS, Guenther FH. White matter impairment in the speech network of individuals with autism spectrum disorder. Neuroimage Clin 2013;3:234–241.
27. Gotts SJ, Simmons WK, Milbury LA, Wallace GL, Cox RW, Martin A. Fractionation of social brain circuits in autism spectrum disorders. Brain 2012;135(Pt 9):2711–2725.
28. Solomon M, Ozonoff SJ, Ursu S, et al. The neural substrates of cognitive control deficits in autism spectrum disorders. Neuropsychologia 2009;47(12):2515–2526.
29. Xiao Z, Qiu T, Ke X, et al. Autism spectrum disorder as early neurodevelopmental disorder: evidence from the brain imaging abnormalities in 2-3 years old toddlers. J Autism Dev Disord 2014;44(7):1633–1640.
30. Catani M, Dell'Acqua F, Budisavljevic S, et al. Frontal networks in adults with autism spectrum disorder. Brain 2016;139(Pt 2):616–630.
31. Casey BJ, Somerville LH, Gotlib IH, et al. Behavioral and neural correlates of delay of gratification 40 years later. Proc Natl Acad Sci U S A 2011;108(36):14998–15003.
32. Leh SE, Ptito A, Chakravarty MM, Strafella AP. Fronto-striatal connections in the human brain: a probabilistic diffusion tractography study. Neurosci Lett 2007;419(2):113–118.
33. Wang J, Wang L, Zang Y, et al. Parcellation-dependent small-world brain functional networks: a resting-state fMRI study. Hum Brain Mapp 2009;30(5):1511–1523.